Journal of *Marine Science and Engineering*

MDPI

Article

Investigating Human Influence on Offshore Terrestrial Organic Carbon Trends in a High-Energy Delta: The Ayeyarwady Delta, Myanmar

Evan R. Flynn and Steven A. Kuehl *

Virginia Institute of Marine Science, William & Mary, P.O. Box 1346, Gloucester Point, VA 23062, USA; erflynn@vims.edu

* Correspondence: kuehl@vims.edu

Abstract: The continental margin is a major repository for organic carbon; however, anthropogenic alterations to global sediment and particulate terrestrial organic carbon (TerrOC) fluxes have reduced delivery by rivers and offshore burial in recent decades. Despite the absence of mainstem damming, land use change in the Ayeyarwady and Thanlwin River catchments in Myanmar has accelerated over the last 50 years. As a result, deforestation and landscape erosion have likely altered fluvial fluxes to the Northern Andaman Sea shelf; however, the magnitude and preservation of geochemical signals associated with development are unknown. Utilizing elemental and bulk stable and radioisotope analysis, this study investigates spatial and temporal trends in sediment sources and TerrOC concentrations to identify the potential impacts of recent (<100 years) offshore development. While our results demonstrate an along-shelf trend in provenance and TerrOC concentrations, temporal (downcore) trends are not observed. We attribute this observation to frequent, large-scale seabed resuspension and suggest that extensive mixing on the inner shelf creates a low-pass filter that effectively attenuates such signatures. This is in contrast to other large Asian deltas, where signals of human landscape disturbance are clearly preserved offshore. We predict that planned mainstem damming in Myanmar will result in larger alterations in sediment and TerrOC supply that may become apparent offshore in the near future.

Keywords: terrestrial organic carbon; continental shelf; human impacts; Ayeyarwady River Delta; macrotidal; sediment resuspension

Received: 5 December 2024
Revised: 13 January 2025
Accepted: 16 January 2025
Published: 18 January 2025

Citation: Flynn, E.R.; Kuehl, S.A. Investigating Human Influence on Offshore Terrestrial Organic Carbon Trends in a High-Energy Delta: The Ayeyarwady Delta, Myanmar. *J. Mar. Sci. Eng.* **2025**, *13*, 163. https://doi.org/10.3390/jmse13010163

1. Introduction

Large river deltas provide invaluable ecologic and economic resources to the human populations that inhabit them, and thus, many delta plains have been extensively modified to support coastal communities through urban, agricultural, navigational development, and more [1–6]. This includes, for example, the utilization of river control structures, damming, water diversion for irrigation, mining, and deforestation throughout river catchments, all of which impact the sediment and particulate terrestrial organic carbon (hereafter TerrOC) loads carried by rivers [3,5,7–10]. While some of these activities promote sediment and TerrOC retention on the terrestrial landscape (e.g., reservoirs, water diversions), others serve to promote erosion (e.g., deforestation, mining) [3,5,7,11]. In combination, humans have driven a 2300 ± 600 Mt y^{-1} increase in global fluvial sediment movement across landscapes, primarily due to deforestation, while simultaneously decreasing global delivery to the ocean by 1400 ± 300 Mt y^{-1} through reservoir retention [7].

The delivery of TerrOC to the global ocean is closely linked to sediment fluxes as organic carbon binds to fine-grained sediments (i.e., mud, or <63 μm), resulting in a dominant sedimentological control over transport and reactivity [10,12–16]. In river catchments, TerrOC is processed as it undergoes periods of resuspension and deposition through river-floodplain exchange [13,17]. Because TerrOC is also derived from fluvial primary production, rivers often exhibit complex TerrOC mixtures with a wide range of ages and reactivities [10,13,14]. Altering river catchments can thus greatly impact the quantity and quality of TerrOC fluxes [3,10]. For instance, sediment fluxes in Asian rivers have been reduced in proportion to the number of large dams in a catchment [8,18]. The settling and sequestration of material in reservoirs behind dams also alters the flow of essential nutrients to the coastal ocean and can drive an increase in primary productivity upstream [19].

Terrestrial deforestation and mining serve to decrease soil organic carbon content and increase the delivery of fine sediment to the coastal ocean [10,20,21]. River control structures, such as levees and weirs, increase the flux of relatively undegraded TerrOC to the ocean by limiting river-floodplain exchange [9,10,18]. In Changjiang, for example, the effects of development are reflected in changes in fluvial C/N ratios and $\delta^{13}C$ that suggest larger contributions of phytoplankton productivity due to reduced sediment loads from damming [22]. In contrast, using $\delta^{13}C$ and radiocarbon, a study on the Pearl River attributed a ~140% increase in petrogenic TerrOC fluxes since the 1970s to accelerating dam construction and likely to coal consumption [18].

In tropical and subtropical deltas, reduced freshwater flow limits the extent of brackish water required for mangrove growth [23]. Because mangroves provide a trap for coastal sediment and TerrOC, floodwater storage, nutrient filtration, and energy dissipation from erosive waves, they are essential to delta sustainability and coastal carbon cycling [3,10,23–26]. As such, the removal of mangroves likely impacts coastal carbon processes as trapping is reduced, and leaf litter and soils are eroded [27–32]. While less well understood, the impacts of mangrove deforestation on marine carbon cycling may be significant, as deforestation and the loss of coastal carbon stocks have been extensive in large deltas with high particle fluxes [26,33–37]. Overall, because deltas sequester nearly 50% of the TerrOC buried in the marine environment, modifications to large rivers likely have a substantial impact on the global carbon cycle [18,38].

The Ayeyarwady and Thanlwin (A-T) are two of Myanmar's largest rivers, discharging a combined ~485 Mt y^{-1} of sediment and ~1.9 Mt y^{-1} of TerrOC onto the Northern Andaman Sea continental shelf [39]. Energetic oceanographic conditions on the inner shelf drive the formation of a muddy subaqueous clinoform, with the top set region extending across the shallow, tidally influenced Gulf of Martaban and seaward progradation of foreset beds into a mid-shelf pull-apart basin known as the Martaban Depression (Figure 1) [40–42]. The shelf also exhibits a region of increased wave energy off the "Mouths of the Ayeyarway", as well as a mud drape on the NW shelf (Figure 1) [40–42]. Tidally driven sediment resuspension in the Gulf of Martaban may facilitate the partial oxidation of TerrOC prior to accumulation on the shelf [40,42,43]. In contrast, TerrOC content is highest in modern deposits on the NW shelf, which derives its sediment from small rivers of the Indo-Burman Range (IBR) [42,44].

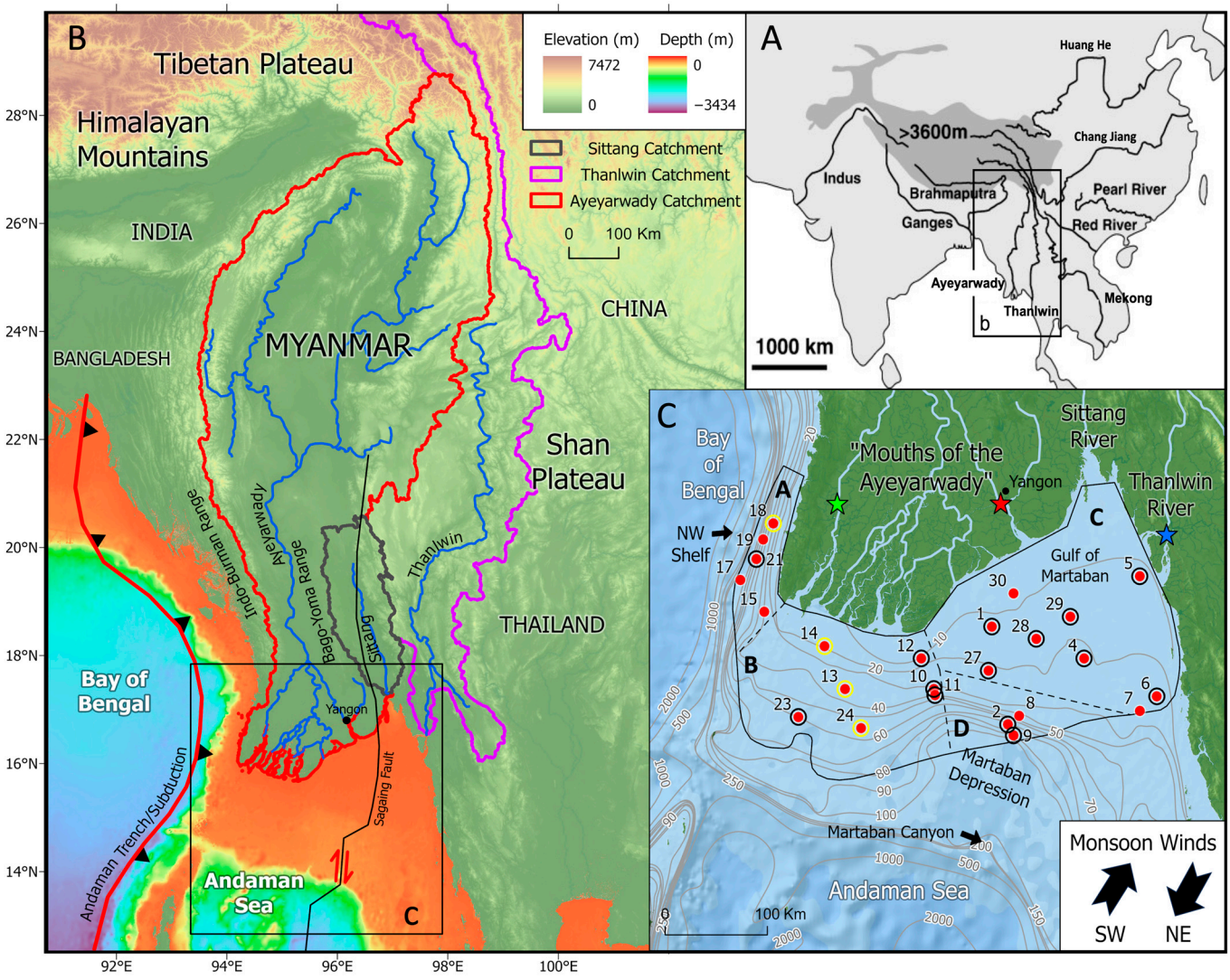

Figure 1. Reference and core location maps for the Ayeyarwady Delta, Myanmar: (**A**) Ayeyarwady and Thanlwin Rivers along with other major rivers in Asia; (**B**) Andaman Sea bathymetry and regional tectonic setting (Bathymetry from [45]); (**C**) Study area with coring sites from [40] (red circles) and Pathein, Yangon, and Thanlwin river sampling locations from [40,46] (indicated by green, red, and blue stars, respectively). Black circles around coring sites indicate that no ^{7}Be was detected in surface sediment, whereas yellow circles indicate the presence of ^{7}Be. The region of modern sediment accumulation on the shelf is indicated by the black polygon [42]. Depositional regions are separated by dashed lines into (**A**) the NW shelf, (**B**) "Mouths of the Ayeyarwady", (**C**) the Gulf of Martaban, and (**D**) the Martaban Depression. Smoothed bathymetric contours (gray lines) are shown in meters of water depth (adapted from [45]).

Unlike many Asian river deltas, the A-T rivers have remained relatively undeveloped due to an extended period of political and economic isolation in Myanmar and a current lack of mainstem damming [11,33,47]. Nonetheless, in the last 50 years, anthropogenic impacts have increased with the expansion of industries such as agriculture and mining [11,48]. In the Ayeyarwady catchment, several studies have already identified alterations to shoreline morphology due to land use change [11,48]; however, the effects on sediment provenance and TerrOC content offshore remain unclear. With development expected to continue in the A-T catchments, an understanding of the connection between fluvial fluxes and offshore accumulation is of increasing importance. Here, we aim to address these gaps in knowledge by utilizing stable and radioisotopes, a binary mixing model, and elemental analysis to investigate potential changes in sediment provenance and TerrOC content in

the offshore Ayeyarwady delta over the last 100 years. Spatial trends in organic carbon and source-specific elemental ratios on the shelf are explored to determine the dispersal patterns of sediment from contrasting fluvial sources. Comparing our findings to other large, developed river deltas, we then explore why some river–ocean margin systems preserve signals of human perturbations while others may not.

2. Study Area

2.1. Regional Climate and Oceanographic Conditions

The Ayeyarwady delta region lies in a monsoonal climate where SW and NE monsoon winds drive seasonally reversing surface currents on the Northern Andaman Sea continental shelf (Figure 1) [49]. Despite such seasonality, recent modeling efforts indicate that most of the sediment discharged at the "Mouths of the Ayeyarwady" is transported into the Gulf of Martaban by near-bed currents throughout the year [50]. Macrotidal conditions on the shelf, with semidiurnal tides with M2 (principal lunar) and S2 (principal solar) major components, produce a local tidal range of 4–7 m [51]. In the Gulf of Martaban, tidal currents that reach up to 3 m s^{-1} drive sediment resuspension and produce the world's largest zone of perennial turbidity, spanning > 45,000 km^2 during spring tides [51].

2.2. Ayeyarwady and Thanlwin Rivers

The Ayeyarwady River flows from Himalayan glaciers in Northern Myanmar to the subaerial delta (Figure 1) [52]. With a catchment dominated by metamorphic and plutonic bedrock, ophiolites, and Holocene lavas, Ayeyarwady sediments have an increased abundance of Ni and Cr compared to other large rivers east of the Ayeyarwady catchment, including the Mekong and Chao Phraya [44,52–59]. Aluminum and Fe content in Ayeyarwady sediment is also almost double that of the Thanlwin because of increased weathering and abundance of ferromagnesian rocks in the mafic lithologies [44].

Recent increases in economic activity have led to further development of the Ayeyarwady catchment [11,48,60,61]. In the upper catchment, metal (e.g., Ag, Cu, and Au) and coal deposit mining has resulted in deforestation and reduced river water quality [60]. Similar to other large Asian rivers, legal and illegal sediment mining has also become increasingly prevalent on the river mainstem, driving reductions in coarse grain sediment loads and localized erosion along the western shoreline [11,48,62]. Land conversion from mangrove forests to agricultural fields and aquaculture ponds has also increased in the delta plain, with a notable 52% loss in mangrove cover nationwide between 1996 and 2016 (net loss of 2.5×10^5 ha) [11,33,48,61,63]. In contrast to sediment mining, mangrove deforestation has caused an increase in fine sediment fluxes, resulting in localized accretion on the eastern shoreline [11,48]. Given recent rates of deforestation and the mean belowground carbon stock measured in the Kanhlyashay Natural Mangrove Forest near Yangon (36.73 ± 19.00 Mg C ha^{-1} [64]), we can estimate that as much as 0.69 Mt C yr^{-1} may be lost due to mangrove deforestation. This estimate is over a third of the rivers' TerrOC discharge [39], indicating that delta plain mangrove deforestation may impact fluvial TerrOC fluxes and offshore accumulation. While damming is currently only limited to tributaries, there are plans to install large hydropower dams on the Ayeyarwady mainstem in the coming years, risking a substantial reduction in sediment loads [8,47,60,65].

Rising in the Tibetan Plateau, the Thanlwin River drains igneous bedrock and the largely sedimentary Shan Plateau before discharging from two closely spaced distributaries into the Gulf of Martaban (Figure 1) [44,54,56,57,66]. Due to its steep catchment and highly resistant bedrock, the Thanlwin produces a sediment load of just ~159 Mt y^{-1} compared to the ~326 Mt y^{-1} of the Ayeyarwady [39,49,67]; however, both rivers have a similar TerrOC load of ~1 Mt y^{-1}. The Sittang River, located between the A-T rivers (Figure 1), transports

sediment with a composition similar to that of the Thanlwin [68] and, along with other small rivers, may deliver an additional 50 Mt y^{-1} of sediment and an unknown quantity of TerrOC to the Gulf of Martaban [69].

Unlike the Ayeyarwady, the Thanlwin is a transnational river flowing through China, Thailand, and Myanmar, making catchment regulations challenging [70,71]. Mining (e.g., Sb, Pb, and Zn) and illegal logging in the catchment have caused extensive deforestation and soil erosion [70–73]. Sediment mining has also recently increased in the lower reaches of the river [70]. Despite the current lack of mainstem damming, hydropower projects have been proposed by China, Thailand, and Myanmar, which would result in significant fragmentation of the river and reduced sediment fluxes [70].

2.3. Holocene Progradation and Modern Offshore Accumulation

The Ayeyarwady delta plain formed over the mid-to-late Holocene, with subaerial progradation occurring until the delta front reached the southernmost extent of the subaerial IBR [59]. The increased focus of wave energy on the emerging headland has since kept the subaerial delta front in a state of relative equilibrium for the last ~150 years [59,74]. Without modern subaerial growth, fluvial sediment is largely exported offshore, with an estimated 70–80% of the A-T sediment load being retained on the shelf [42,59].

The shallow (<30 m), macrotidal Gulf of Martaban receives a majority of the A-T sediment flux and is characterized by deep (up to 1 m) seabed mixing, limited accumulation, and the formation of fluid muds with near-bed turbid layers extending 2–11 m above the seabed [40,42,43]. Surficial sediment provenance also suggests that the Gulf of Martaban contains a homogenous mixture of A-T river sediment [44]. From the Gulf of Martaban, sediment is transported seaward to the Martaban Depression, likely via tidal currents and/or storm-driven gravity flows [41–43,51]. The Martaban Depression is the primary depocenter for sediment on the shelf, with offshore accumulation rates reaching as high as ~6 cm y^{-1} in foreset beds [38,40]. Because the southern extent of the Martaban Depression only exhibits relict sands, the transport of deltaic mud to the deep sea via the Martaban Canyon likely does not occur at the present sea level highstand [40,41].

Offshore of the "Mouths of the Ayeyarwady", the most substantial accumulation occurs in a narrow, nearshore mud belt (<40 m water depth), while the rest of the 50,000 km^2 ramp-like shelf region exhibits a mixture of modern and relict sands with relatively low accumulation rates (<1 cm y^{-1}) [40,42,75]. Low accumulation on the outer shelf is attributed to frequent fine sediment resuspension by large swells from the Bay of Bengal [40,51,75].

The NW shelf is characterized by a ~20 m-thick Holocene mud drape that extends over the shelf break, indicating the potential for shelf escape into the deep Bay of Bengal [40,41]. Accumulation rates in the region are moderate at ~1 cm y^{-1} [40,42]. In contrast to other regions, small rivers draining the western IBR may also provide a significant source of sediment to the NW shelf [44,76,77]. However, the elemental composition of IBR sediment is unknown. Core X-rays from the NW shelf also show fine and coarse grain layers with sharp basal contact, which may represent storm deposits [40].

3. Methods

3.1. Sample Collection

This study leverages a suite of 25 Kasten cores and 14 gravity cores that were collected from the offshore Ayeyarwady delta as a part of an interdisciplinary research cruise in December 2017 (Figure 1) [40]. As described below, Kasten cores were utilized for isotope, grain size, and surface area analysis, and gravity cores for elemental analysis. Kasten and gravity cores were collected at the same coring locations during the 2017 cruise. However, gravity cores were not recovered from all sites. River grab samples collected from the

Yangon and Pathein distributaries of the Ayeyarwady and the mouth of the Thanlwin (Figure 1) [40,46] were utilized for elemental end-member analysis. Detailed descriptions of the methods and data collection for all samples are reported in [40,46].

3.2. Isotope and Organic Elemental Analysis

^{210}Pb data previously reported in [42] were used to guide organic carbon sample selection. The majority of samples were selected from predetermined geometric intervals (i.e., [40]) within the range of excess ^{210}Pb decay (indicating deposition in the last 100 years). When a surface mixed layer (SML) was indicated by uniform excess ^{210}Pb activities at the core top [42], a near-surface sample in the SML was selected for analysis. In cores that reached undetectable levels of excess ^{210}Pb (i.e., >100 years old), a sample directly below the range of excess ^{210}Pb decay was also selected for analysis. ^{7}Be, another short-lived radioisotope with a half-life of 53.3 days, was measured via gamma spectroscopy to identify areas of recent fluvial input based on the presence or absence of ^{7}Be activity (e.g., [78]). For analysis, samples were dried, ground, packed into Petri dishes, and counted for 24 h on germanium gamma counters to identify ^{7}Be photopeaks at 477.7 keV.

Stable carbon and nitrogen isotope analysis was conducted on 108 samples from 24 of the Kasten cores, with three to six samples being analyzed per core depending on the core length and sample availability. Samples (~20 mg) were weighed into double-layered tin capsules, acidified, and pelletized. All samples were run in duplicate. Acidification followed methods presented in [42], including the stepped, dropwise addition of 1N HCl with a 24 h reaction time, followed by a 24 h drying period in an oven at 60 °C. Prepared samples were run on an Elementar Vario MICRO cube elemental analyzer interfaced to a Sercon Europa 20-20 IRMS at the UC Davis Stable Isotope Facility to identify total organic carbon (TOC), total nitrogen (TN) and carbon and nitrogen stable isotopes (δ^{13}C and δ^{15}N, respectively). Samples were measured relative to international standards, including VPDB and atmospheric N_2 for δ^{13}C and δ^{15}N, respectively. Precision, determined through replicate analysis of internal standards, was high at ±0.09‰ for both δ^{13}C and δ^{15}N. Of all duplicates analyzed, 100 samples had TN ≤ 20 µg, and 17 had TOC ≤ 100 µg, resulting in a precision decrease as TOC and TN approached values similar to the lowest TOC and TN of reference material. Nonetheless, reproducibility between duplicates remained relatively high with average standard deviations of ±9.35 µg for TOC, ±0.260‰ for δ^{13}C, ±1.10 µg for TN, and ±0.159‰ for δ^{15}N. Samples that contained less TOC or TN than the reference material were excluded from TerrOC data analysis due to the decreased accuracy of the analytical measurement. This included KC-07 (80–82 cm), KC-12 (60–61 cm), KC-13 (32–34 cm), KC-13 (60–62 cm), KC-14 (80–82 cm), and KC-23 (30–32 cm). Cores with less than three remaining downcore samples were also not utilized (i.e., KC-07, KC-12, KC-13, and KC-23).

3.3. Surface Area and Grain Size

Surface area was determined for all samples using a Micrometrics Gemini V Surface Area and Pore Size Analyzer. Following methods in [79], ~1 g of freeze-dried sediment was weighed into crucibles for combustion at 350 °C for 12 h to remove organic matter. Samples were then degassed for 0.5 h on a Micrometrics FlowPrep 060 at 200 °C to remove the water before being measured by the five-point Brunauer, Emmett, and Teller (BET) method [80]. To determine instrument accuracy, a kaolinite standard was run each day the instrument was operated. BET error for all samples was low at an average of ±0.064 m^2 g^{-1}.

For grain size, datasets previously reported in [40,42] were supplemented with newly collected data (N = 19) to provide a direct comparison between grain size and stable isotope data where possible. Because offshore samples have substantial silt and clay size

fractions [40,42], only wet or freeze-dried samples were used for additional grain size analysis [81]. Therefore, comparison was only possible for around half of the samples analyzed for stable isotopes (N = 52). Sample preparation included the addition of ~10 mL of 10% sodium hexametaphosphate solution, vortexing, and letting samples rest for at least 12 h prior to analysis. To ensure complete disaggregation of fine grains, all samples were also sonicated using a Misonix Sonicator 3000 (Misonix, Farmingdale, NY, USA) for 1–2 min before being analyzed on a Beckman Coulter LS 13-320 (Beckman Coulter, Brea, CA, USA). Individual samples were run in triplicate, and size fractions were measured as a percentage by volume binned into 93 intervals between <0.375 and 2000 μm. Triplicate runs were averaged to produce D_{50}, D_{90}, and mud content (percent binned into <16 μm) for each sample.

3.4. X-Ray Fluorescence (XRF) Elemental Analysis

Elemental analysis was conducted on all gravity cores and river end-member samples using an ITRAX XRF Corescanner at the Large Lakes Observatory, XRF Core Scanning Facility. Split gravity cores were scanned at 1 cm resolution for detectable elements ranging from Mg (atomic number 12) to Bi (atomic number 83). River end-member samples, on the other hand, were dried, ground, and packed into 1 × 1 cm cubes for scanning. Elemental abundance was provided in counts per second (cps), which was normalized to coherent scatter for comparison between wet gravity cores and dried river samples. However, in this study, our use of elemental ratios largely precludes the necessity of such normalization.

4. Results and Discussion

4.1. Spatial Organic Carbon Trends

TerrOC content was estimated using a simple, binary $\delta^{13}C$ mixing model (Equation (1); [42]) with regional marine (−20.5‰) and terrestrial (−25.1‰) end-members as identified in [82,83], respectively. While we acknowledge that binary mixing models have the potential to be limited in application due to the range of $\delta^{13}C$ values associated with various TerrOC sources (i.e., freshwater algae, C_3 and C_4 terrestrial plants [84]), such calculations can be highly valuable in providing a first-order approach to estimating TerrOC content through well-established bulk sediment analysis methods. For this study, the percent TerrOC derived from Equation (1) is further converted to wt.% using the TOC mass and sample weight, which can be found in Table S1. Moreover, due to the limited number of samples that contained >10–20 mg TN (see Section 3.3) and evidence of additional nitrogen cycling offshore, we elected not to use $\delta^{15}N$ and N/C-based mixing models for TerrOC estimates [42,85–88].

$$\frac{\left(\delta^{13}\text{C Marine end-member}\right) - \left(\delta^{13}\text{C Observed}\right)}{\left(\delta^{13}\text{C Marine end-member}\right) - \left(\delta^{13}\text{C Terrestrial end-member}\right)} = \textit{Estimated \% TerrOC} \quad (1)$$

For spatial analysis, discrete values in each core were averaged and plotted in ArcGIS. Overall, core-averaged TOC increases from north to south in the Northern Andaman Sea, while core-averaged TerrOC generally decreases from north to south (Figure 2). Low TOC content at the head of the Gulf of Martaban is likely due to increased turbidity on the inner shelf [67]. However, as light availability increases on the outer shelf, higher levels of marine primary productivity may drive the higher TOC content observed in the Martaban Depression (Figure 2) [67,89]. In contrast, based on bulk stable isotopes, TerrOC concentrations decrease from the Gulf to the Depression (Figure 2), showing a similar distribution to findings from [42], which also utilized bulk stable isotopes and a binary mixing model to assess TerrOC content on the Northern Andaman Sea shelf. While

both [42] and this study provide first-order approximations through bulk analyses, such results demonstrate the potential for loss of TerrOC components across the shelf, which could be attributed to extended residence time in oxidative resuspension–deposition cycles in the Gulf of Martaban [13,14,40,41]. Both TOC and TerrOC content increase from east to west along the Northern Andaman shelf, with the highest core-averaged TOC and TerrOC content being found on the NW shelf (Figure 2). In fact, TerrOC makes up the majority of the TOC (~60–70%) in the region. Such high proportions of terrestrial material could suggest that the NW shelf has a higher supply of TerrOC compared to other regions and/or that material delivered to the NW shelf is minimally, if at all, processed prior to deposition. Because additional TerrOC input from streams draining the IBR is probable [44], an increase in TerrOC supply to the NW shelf from local rivers may contribute to the observed increase in concentration. This is consistent with previous lignin analysis in surface sediments reported in [41], where lignin was found to be more preserved on the NW shelf compared to more degraded in the tidally mixed Gulf of Martaban.

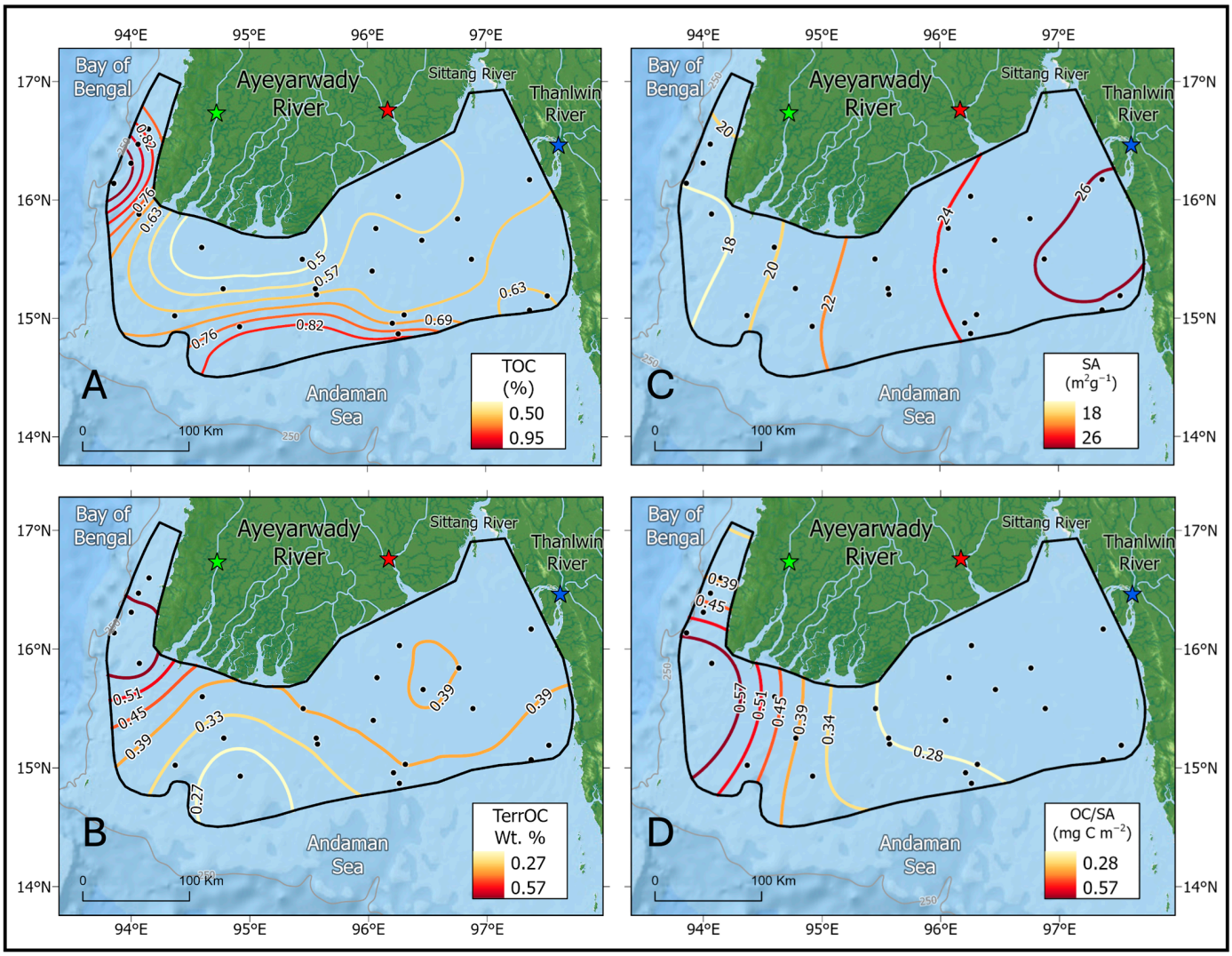

Figure 2. Core-averaged organic carbon and surface area results including (**A**) TOC (%), (**B**) TerrOC wt.%, (**C**) surface area (SA), and (**D**) organic carbon loading (OC/SA). Coring locations are shown as black circles. Locations of Pathein, Yangon, and Thanlwin river end-members are shown as green, red, and blue stars, respectively. The black polygon indicates the region of modern sediment accumulation as defined in [42].

The spatial distribution of SA is similar to mud content previously reported in [40,42], both being lowest on the NW shelf (Figure 2). This is likely a result of changing depositional environments offshore, with wave energy promoting the winnowing of fine grains on the western shelf and tidal cycles keeping fine grains in suspension in the Gulf of Martaban [40,41,43,50].

Core-averaged organic carbon loading (OC/SA) is also highest on the NW shelf and lowest in the Gulf of Martaban and Martaban Depression (Figure 2). This east-to-west trend has a slight correlation to grain size (i.e., D_{90} and mud content), as lower mud content and higher D_{90} are associated with the highest OC/SA in the few cores on the NW shelf, while relatively higher mud content and lower D_{90} are associated with the lowest OC/SA in the Gulf of Martaban and Martaban Depression (Figure 3). While not generally expected, the relatively high OC/SA and coarser grains on the NW shelf may be explained by either high OC/SA in small IBR rivers or a regional increase in abundance of marine OC. Having small catchments with high relief, small mountainous rivers discharge high sediment fluxes with large quantities of relatively undegraded TerrOC [38]. While we cannot rule out potential addition of marine OC through primary production, because OC/SA observed on the NW shelf is similar to other mountainous rivers (0.4–1 mg C m^{-2}) [13,90], and the majority of the TOC in the region is of terrestrial origin, OC/SA is most likely driven by high TerrOC content. By comparison, the average OC/SA in the Gulf of Martaban and Martaban Depression is much lower and more similar to that found in large deltas such as the Amazon and Chang Jiang (~0.2 mg C m^{-2}) due to energetic and oxidative oceanographic conditions on the proximal subaqueous delta topsets [13,91,92] (Figures 2 and 3). While we do observe a slight across-shelf increase in OC/SA from the Gulf of Martaban to the Martaban Depression, this is attributed to marine OC replacement, which has also been identified offshore the Chaing Jiang delta through $\delta^{13}C$ enrichment [92].

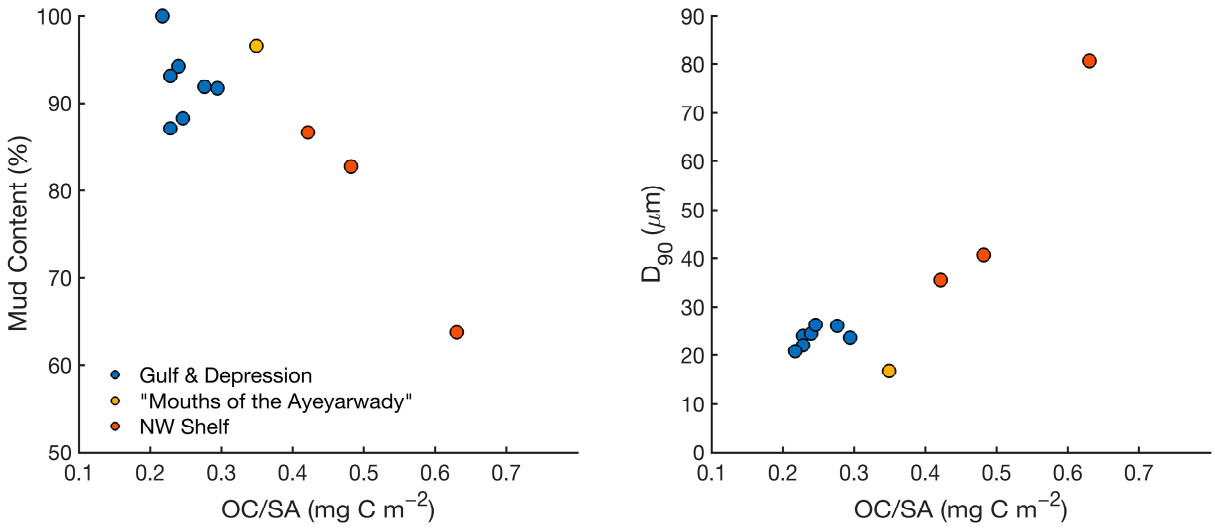

Figure 3. Organic carbon loading (OC/SA) plotted in relation to grain size parameters for each of the offshore regions with the Gulf and Depression shown in blue, "Mouths of the Ayeyarwady" in yellow, and the NW shelf in red.

4.2. Temporal Organic Carbon Trends

Despite increased land use changes in the A-T catchments over the last 50 years, organic carbon and grain size parameters (i.e., TOC, $\delta^{13}C$, SA, D_{50}, D_{90}, and mud content) exhibit no substantial downcore variation in the offshore sediment record (Figures 4 and 5). Across all cores analyzed, the average downcore change in TOC, $\delta^{13}C$, and TerrOC was minimal at 0.044%, 0.29‰, and 0.012 wt.%, respectively. Notably, the change in TerrOC

content was half the average analytical error (±0.024). Although not used for TerrOC estimates, nitrogen also demonstrated minimal downcore variation with an average downcore change of 2.62 mg TN and 0.099‰ $\delta^{15}N$ and no significant variability in N/C. While downcore SA showed a slight correlation with D_{90}, there is minimal change in all grain size parameters (D_{50}, D_{90}, and mud content) when SA is >20 m^2g^{-1} (Figure 6). Therefore, we find no significant or consistent change in SA, grain size, or OC/SA with depth (Figure 5).

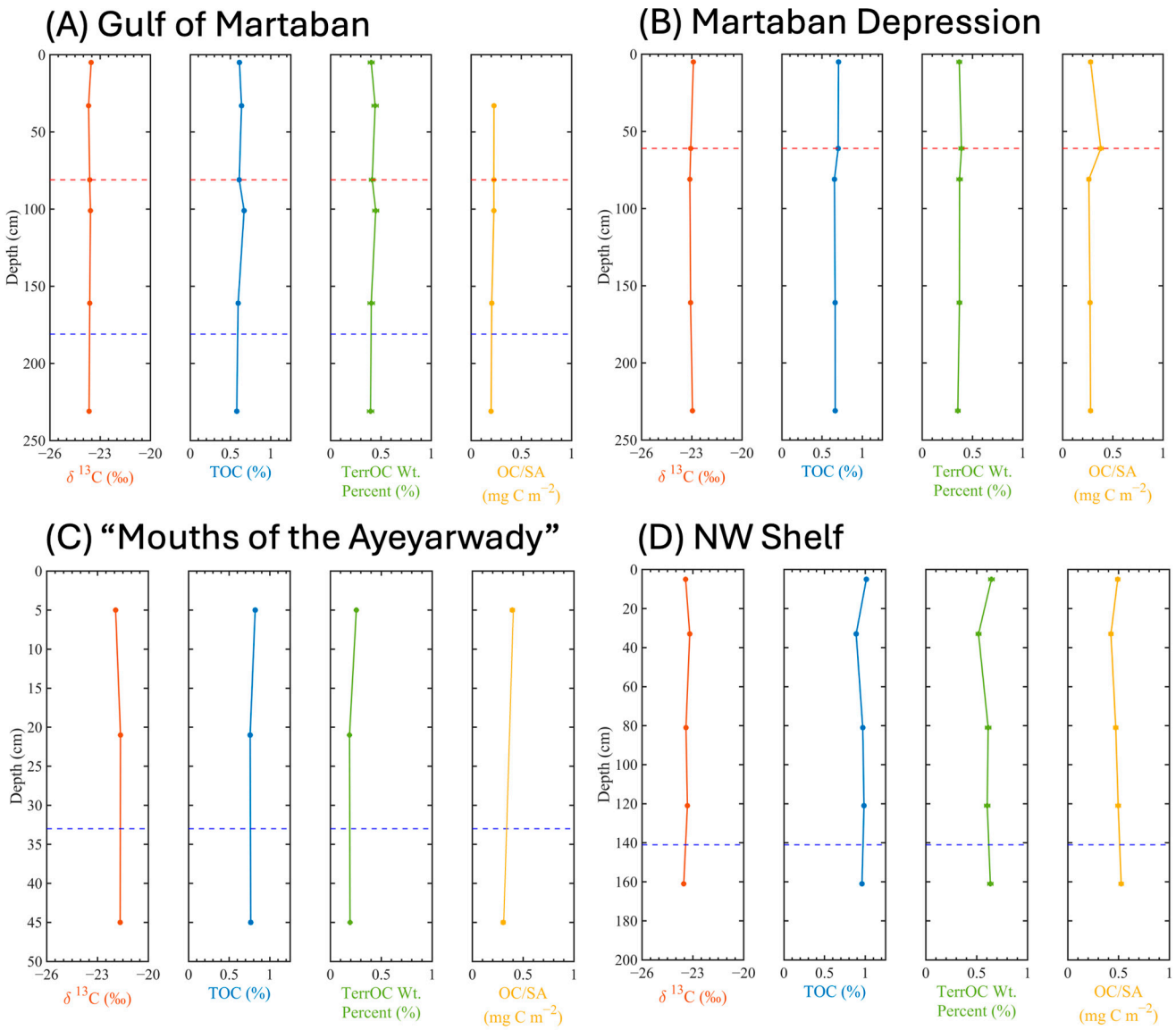

Figure 4. Example downcore plots of $\delta^{13}C$, TOC, TerrOC, and OC/SA from the (**A**) Gulf of Martaban (KC-04), (**B**) Martaban Depression clinoform forests (KC-02), (**C**) "Mouths of the Ayeyarwady" (KC-24), and (**D**) NW shelf (KC-21). Red dashed lines indicate the depth of the SML, and blue dashed lines indicate the depth at which excess ^{210}Pb is no longer detectable. Overall, cores from all regions demonstrate a lack of downcore change with relatively consistent $\delta^{13}C$, TOC, TerrOC, and OC/SA at depth. Organic carbon data for all cores can be found in Table S1.

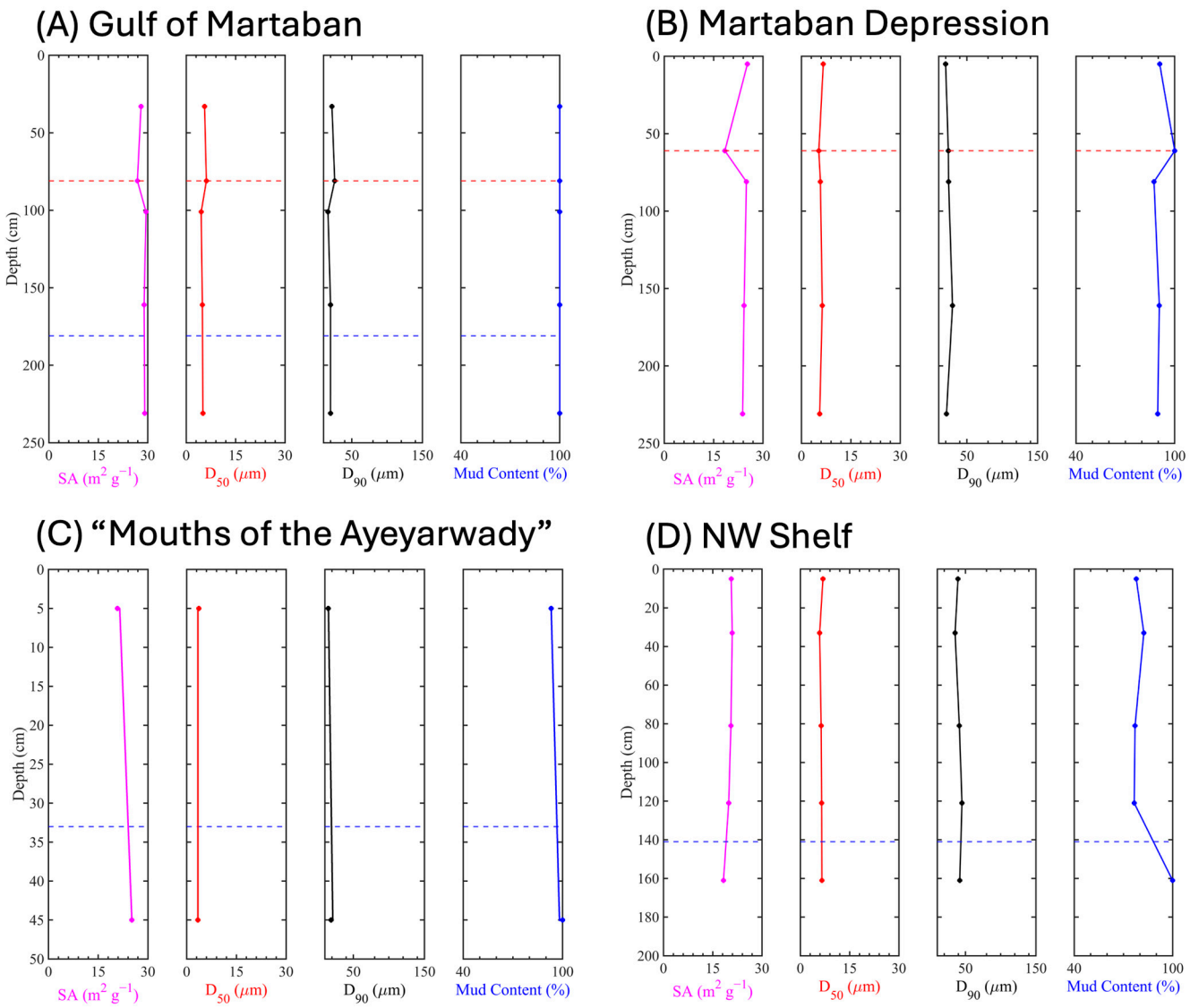

Figure 5. Example downcore plots of surface area (SA), D_{50}, D_{90}, and mud content (%) from the (**A**) Gulf of Martaban (KC-04), (**B**) Martaban Depression clinoform forests (KC-02), (**C**) "Mouths of the Ayeyarwady" (KC-24), and (**D**) NW shelf (KC-21). Red dashed lines indicate the depth of the SML, and blue dashed lines indicate the depth at which excess ^{210}Pb is no longer detectable. SA and grain size for all cores can be found in Tables S2 and S3, respectively.

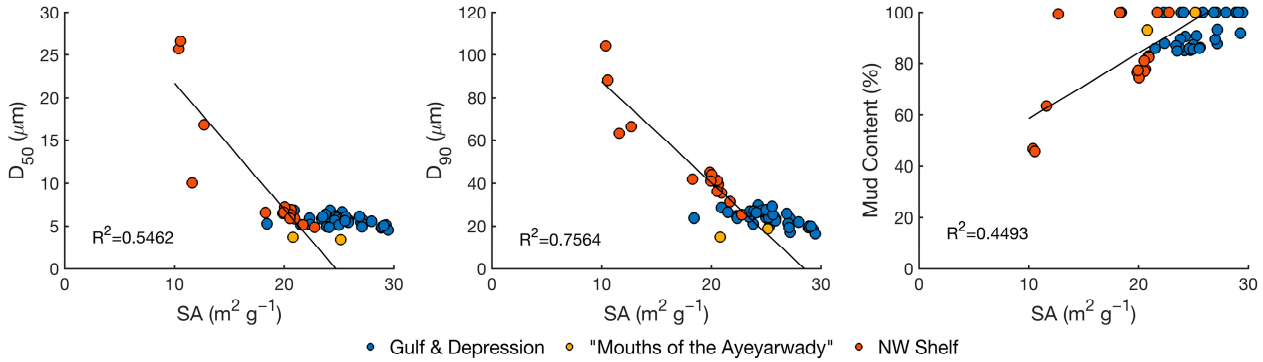

Figure 6. Correlations between surface area (SA) and grain size parameters, including D_{50}, D_{90}, and mud content for all sediment samples analyzed. D_{90} exhibits the strongest correlation with SA;

however, all grain size parameters show minimal change once SA reaches over 20 m^2g^{-1}. Depositional regions are indicated by color, with the Gulf and Depression shown in blue, "Mouths of the Ayeyarwady" in yellow, and the NW shelf in red.

The lack of temporal (downcore) variation in TerrOC content on the Northern Andaman shelf can either be explained by constant fluvial fluxes and/or the low-pass filtering of geochemical signals through frequent seabed resuspension. Because changes to the Ayeyarwady sediment load in recent years have already been identified [11,48], we argue that frequent seabed resuspension effectively creates a low-pass filter for modern signals of changing fluvial fluxes by increasing residence time and, to a lesser extent, oxidizing terrestrial material. In this case, tidally and seasonally driven resuspension and exchange of material between the turbid water column, fluid muds, and SML keeps much material in suspension for extended periods of time [93,94], during which TerrOC may also be processed through increased oxygen exposure.

We can explore the impacts of increased residence time on geochemical signals using the distribution of ^{7}Be activity in surface sediments (Figure 1 and Table S4). Because ^{7}Be is a short-lived radioisotope derived from atmospheric fallout and commonly associated with the flux of fresh riverine sediment to the ocean (e.g., [78]), we would expect ^{7}Be to be present in the Gulf of Martaban. However, ^{7}Be is not detected in the Gulf of Martaban, suggesting that frequent resuspension and massive dilution render levels of ^{7}Be below the detectable limit. Moreover, because frequent seabed resuspension and oxidative conditions within the water column may effectively remineralize TerrOC, limiting accumulation to the most recalcitrant and/or mineral aggregate-protected components as has been seen in the Amazon, Chang Jiang, and Huang He [91,92,95–98], changes to fluvial fluxes associated with increased labile TerrOC loads may not be observed due to rapid and/or extensive oxidation prior to accumulation. While it may also be possible that accumulation rapidly moves material through the diagenetic zone of the seabed, we do not find a relationship between changes in downcore TerrOC content or OC/SA and accumulation rate (Figure 7), further indicating that frequent seabed resuspension provides a low-pass filter for changing fluvial TerrOC fluxes.

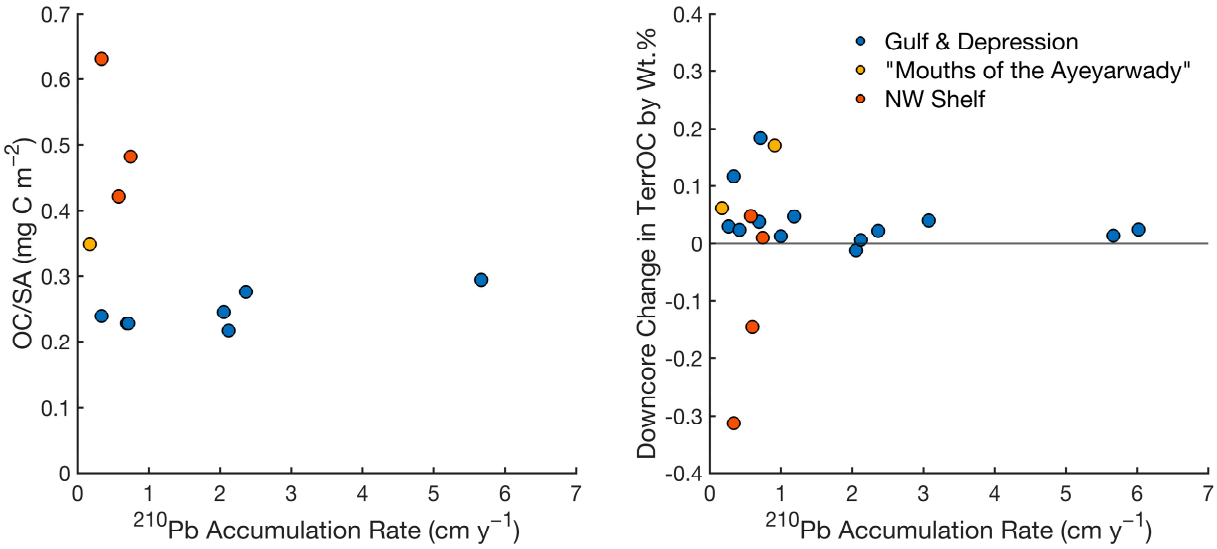

Figure 7. ^{210}Pb accumulation rates plotted in relation to (**Left**) core-averaged OC/SA and (**Right**) average downcore changes in TerrOC by wt.%. Downcore change in TerrOC by wt.% was calculated for each core by subtracting the observed TerrOC wt.% at the bottom of the core from that at the surface. Positive values thus indicate a decrease in TerrOC at depth, while negative values

indicate an increase in TerrOC at depth. In both plots, depositional regions on the shelf are plotted by color, with the Gulf of Martaban and Martaban Depression shown in blue, "Mouths of the Ayeyarwady" shown in yellow, and the NW shelf shown in red.

Although TerrOC is rapidly buried on the NW shelf, no downcore changes are observed (Figure 4). While we do not have data from the streams draining the IBR to determine the regional burial efficiency of TerrOC, the consistent, relatively high downcore TerrOC content and OC/SA suggest effective regional preservation of terrestrial material on the NW shelf, with limited diagenetic alternations occurring based on our bulk isotopes analyses. In contrast to the A-T rivers, rivers in the IBR that likely supply sediment to the NW shelf have much smaller catchments and are minimally populated. Therefore, it is probable that the near-constant temporal trends in organic carbon on the NW shelf are due to minimal development in the IBR and unaltered fluvial TerrOC fluxes.

4.3. Sediment Provenance

To identify A-T fluvial sources, we utilized elemental ratios characteristic of river end-members. XRF analysis indicated that Thanlwin River sediment had relatively higher Rb and Zn content, whereas the Pathein and Yangon distributaries of the Ayeyarwady had relatively more Ni and La, which aligns with the literature on river catchment geology and mineral deposits [57,58,99,100]. We accordingly identified Ni/Rb and Zn/La to be source-specific elemental ratios, with high Ni/Rb and high Zn/La ratios representing Ayeyarwady and Thanlwin sediment, respectively.

Offshore core-averaged Ni/Rb and Zn/La ratios demonstrate prominent east-to-west trends along the Northern Andaman Sea shelf. Overall, the highest average Zn/La ratio is found near the mouth of the Thanlwin in the Gulf of Martaban, while the highest average Ni/Rb ratio is found on the NW shelf (Figure 8). Notably, though, the increase in Ni/Rb and decrease in Zn/La on the NW shelf relative to the ratios proximal to the A-T river mouths indicates the input of sediment from an additional source, such as the IBR (Figure 8). This is supported by similarities in the NW shelf and the Pathein River end-member ratios, as the Pathein likely also receives mafic input from the IBR and has the highest Ni/Rb (0.84) and lowest Zn/La (0.90). Nonetheless, both Pathein ratios are still slightly higher than that observed on the NW shelf. While this could indicate input from the Yangon distributary or the Thanlwin, prevailing easterly near-bed currents and Sr and Nd isotopic ratios suggest that sediment from the Gulf of Martaban and eastern Ayeyarwady distributaries is not transported to the NW shelf [44,50]. Instead, it may be more likely that ratios on the NW shelf are a product of Pathein and local IBR sources, as well as additional sediment delivered to the region by southerly coastal currents [44,101,102].

On the Northern Andaman Sea shelf, Zn/La and Ni/Al ratios both do not vary greatly from mean values downcore, with coefficients of variation being <10%, indicating that sediment sources do not largely vary over time (Figure 9). On the NW shelf, ratio oscillations are slightly more significant, with coefficients of variation being $\leq$10%, with the exception of GC-17, which demonstrates variation of 14% and 20% in Ni/Rb and Zn/La, respectively (Figure 9). The highest variation from the mean Ni/Rb ratio in GC-17 occurs at 15–20 cm, aligning with the presence of intact gastropod shells [40], which suggests that bioaccumulation of heavy metals (e.g., Ni) may drive this observation [103]. Alternatively, increased downcore variation on the NW shelf may be explained by input from Pathein and/or IBR rivers during episodic storm events. In any case, the NW shelf exhibits an increase in the temporal variability of sediment sources compared to the Northern Andaman Sea shelf.

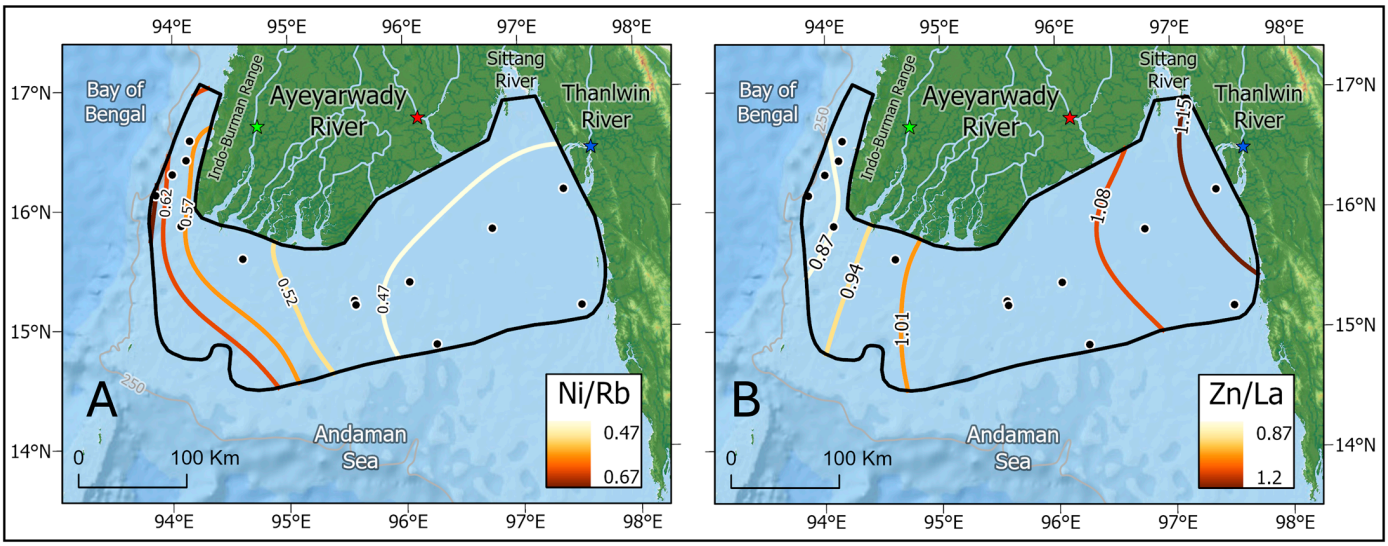

Figure 8. XRF ratios (**A**) Ni/Rb and (**B**) Zn/La are indicative of sediment sources from the Ayeyarwady and Indo-Burman Range and Thanlwin, respectively. Coring locations are shown as black circles, and Pathein, Yangon, and Thanlwin River end-member sample locations are shown as green, red, and blue stars, respectively. The black polygon on the Northern Andaman Sea shelf represents the region of modern sediment accumulation [42].

4.4. Comparing Human Perturbations on High-Energy Margins

Anthropogenic impacts on fluvial TerrOC fluxes have not resulted in observable changes to offshore TerrOC concentrations in the Ayeyarwady delta over the past 100 years; however, in other similarly high-energy Asian deltas, including the Chang Jiang and Huang He, such changes have been observed. In the Chang Jiang, sediment and TerrOC fluxes were reduced with the construction of the Three Gorges Dam in 1985, and as a result, TerrOC accumulation in the proximal subaqueous delta has since decreased by ~97.3% due to the erosion and re-exposure of TerrOC [97]. On the other hand, erosion from the abandoned Huang He delta has increased the flux of refractory, highly degraded TerrOC to the Central Yellow Sea, accounting for 69% of the TerrOC in the region since the 1990s, as input of fresh sediment and TerrOC markedly decreased due to damming [104]. Remobilization of TerrOC in both the Huang He and Chang Jiang emphasizes the importance of knowing the nature and quantity of TerrOC sequestered offshore delta sediments, as reductions to fresh, labile TerrOC inputs and an increase in refractory TerrOC may alter coastal carbon cycling by limiting the oxidation potential of terrestrial material.

In another example, TerrOC fluxes from the less energetic Pearl River delta were reduced after the 1980s due to damming [105]. However, an increase in offshore lignin content indicated that fluxes of vascular plant-derived OC increased primarily due to deforestation during urbanization [105]. This suggests that biomarker analysis can provide further insight into changes in offshore TerrOC content in regions with extensive deforestation. However, differences in hydrodynamics should also be considered. Lower tidal energy reduces physical resuspension offshore of the Pearl River, promoting the preservation of lignin [13]. In contrast, on the Northern Andaman Sea shelf, lignin is degraded during transport, reiterating that hydrodynamics exert a first-order control on TerrOC preservation and can filter signals of anthropogenic impacts offshore of the A-T rivers [41].

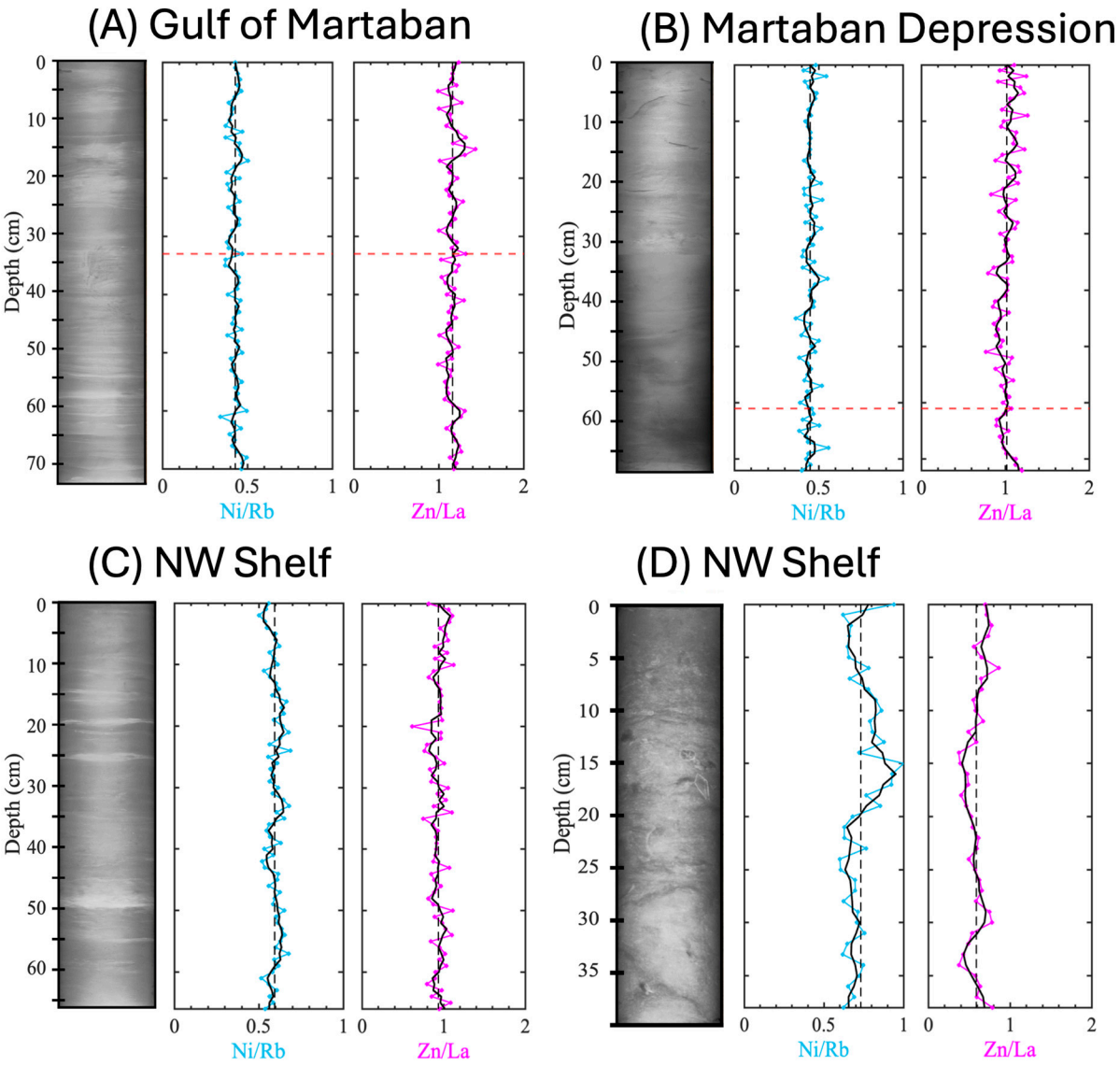

Figure 9. Examples of downcore XRF elemental ratios and core X-rays from the (**A**) Gulf of Martaban (GC-29), (**B**) Martaban Depression (GC-09), and (**C**,**D**) NW shelf (GC-21 and GC-17, respectively). High Ni/Rb ratios (blue) are indicative of sediment sourced from Ayeyarwady distributaries, while high Zn/La ratios (pink) are indicative of sediment sourced from the Thanlwin. 3 cm moving average ratios are plotted for both ratios as solid black lines. Core average ratios are plotted as dashed black lines. Red dashed lines indicate the depth of the SML when present. Core X-ray images are from [40]. XRF ratios for all cores are found in Table S5.

Under high-energy oceanographic conditions, dam construction and reduced fluvial fluxes in the Chang Jiang and Huang He rivers produced signals in shelf sediments, while deforestation and mining in the A-T river catchments did not. The Red and Mekong rivers in Asia have also undergone extensive decreases in fluvial sediment and TerrOC loads due to damming in spite of increasing deforestation [106–108]. In fact, globally, if it were not for dams, rivers would have increased their particulate loads by 212% from 1950 to 2010 [5]. Given the discrepancy between systems impacted by dams and the A-T rivers, we suggest that river connectivity may be a key driver in determining changing fluvial fluxes on TerrOC concentrations in shelf sediments on high-energy margins. While it is challenging to separate the direct effects of individual human impacts (i.e., deforestation, mining, damming, etc.) on fluvial fluxes, dam construction on the Chang Jiang and Huang He rivers has likely impacted fluxes to such an extent that offshore changes are evident

in the sediment record [109–111]. In the case of the Ayeyarwady, however, alterations to sediment and TerrOC fluxes have been largely limited to land use changes that do not directly impact river connectivity [11,47]. The impact of damming and/or other river control structures may be an imperative future consideration for the region as Myanmar faces the potential construction of large dams on the A-T river mainstems [65,71].

5. Conclusions

In this study, we investigated spatial and temporal trends in TerrOC content and sediment provenance off the A-T rivers in association with modern land use changes in the river catchments. Based on short-lived radioisotope geochronology and elemental and stable isotope analyses, we conclude the following:

- Spatial trends in organic carbon and sediment provenance are prominent in an east-west direction along the Northern Andaman Sea shelf, indicating variations in sediment sources and depositional environments between the Gulf of Martaban and Martaban Depression, "Mouths of the Ayeyarwady", and the NW shelf.
- Despite land use changes, no significant temporal (downcore) change in sediment sources or TerrOC contents in shelf sediments has occurred over the last 100 years. On the Northern Andaman Sea shelf, this can be attributed to frequent seabed resuspension, which extends particle residence time and provides conditions necessary for TerrOC oxidation, thereby creating a low-pass filter for signals of changing fluvial fluxes.
- The NW shelf deposit has the highest TerrOC content, which is likely associated with the rapid delivery of TerrOC from small rivers draining the minimally developed IBR. TerrOC preservation on the NW shelf may be increased through efficient burial associated with rapid settling and the formation of episodic storm layers. Deposition across the NW shelf break also suggests that export of TerrOC to the Bay of Bengal via shelf escape is possible, allowing for sequestration over geologic timescales as material undergoes subduction in the Andaman trench.
- Unlike other large, developed Asian rivers, the A-T river mainstems are not obstructed by large dams. Therefore, it is possible that A-T fluvial sediment and TerrOC loads have not yet been impacted to an extent where changes are evident in the offshore sediment record, as has been seen in other large delta systems.

Overall, these findings provide valuable insight into modern spatial and temporal TerrOC trends in the offshore delta as development within Myanmar continues to increase in the coming years. This is especially pertinent as large dams have been planned for both A-T river mainstems, which, if constructed, have the potential to reduce sediment and TerrOC export to the shelf and induce erosion of offshore deposits, as has been seen in other large Asian deltas. Such erosion may release previously sequestered TerrOC, impacting local carbon cycling, as well as increasing coastal instability on the Ayeyarwady delta plain. With 15 million people currently residing on the Delta Plain and depending on the resources it provides, these implications are of critical importance and should be considered in the face of future development.

Supplementary Materials: The following supporting information can be downloaded at: https://www.mdpi.com/article/10.3390/jmse13010163/s1, Table S1: Stable isotope, total organic carbon (TOC), and total nitrogen (TN) data for sediment samples from 24 of the kasten cores located offshore of the Ayeyarwady Delta, Myanmar. Values displayed below indicate an average of duplicate samples; Table S2: Surface area (SA) of available sediment samples from kasten cores collected from the offshore Ayeyarwady Delta, Myanmar; Table S3: Newly collected grain size data for sediment samples from kasten cores collected offshore of the Ayeyarwady Delta, Myanmar; Table S4: Detection

of ^{7}Be in surface samples from a select number of sediment located offshore of the Ayeyarwady Delta, Myanmar. "NP" indicates that ^{7}Be was not detectable within the sample. BC indicates samples from box cores, while KC indicates samples from kasten cores; Table S5: X-ray fluorescence (XRF) elemental data from gravity cores (GC). XRF scans were taken at 1 cm resolution. Elemental ratios Ni/Rb and Zn/La are presented here as sediment provenance indicators for the Ayeyarwady and Thanlwin Rivers, respectively. Raw ratio values and 3-cm moving averages are shown, with moving averages being used to detect variations in source over depth.

Author Contributions: Conceptualization, E.R.F. and S.A.K.; methodology, E.R.F.; writing—original draft preparation, E.R.F.; writing—review and editing, E.R.F. and S.A.K.; funding acquisition, S.A.K. All authors have read and agreed to the published version of the manuscript.

Funding: This research was supported by the National Science Foundation grants OCE-1737221 and OCE-2324953 (PIs S.A. Kuehl and C.K. Harris). Stable isotope analysis, specifically, was funded by institutional student research grants through the Office of Academic Affairs and the Graduate Student Association at the Virginia Institute of Marine Science.

Institutional Review Board Statement: Not applicable.

Informed Consent Statement: Not applicable.

Data Availability Statement: The raw data supporting the conclusions of this article will be made available by the authors upon request.

Acknowledgments: The authors thank faculty and students from the University of Yangon and Mawlamyine University for their support and participation during the December 2017 research cruise that collected the samples analyzed within this study.

Conflicts of Interest: The authors declare that they have no conflicts of interest.

References

1. Syvitski, J.; Saito, Y. Morphodynamics of deltas under the influence of humans. *Glob. Planet. Change* **2007**, *57*, 261–282. [CrossRef]
2. Syvitski, J. Deltas at risk. *Sustain. Sci.* **2008**, *3*, 23–32. [CrossRef]
3. Bianchi, T.S.; Allison, M.A. Large-river delta-front estuaries as natural "recorders" of global environmental change. *Proc. Natl. Acad. Sci. USA* **2009**, *106*, 8085–8092. [CrossRef] [PubMed]
4. Syvitski, J.; Kettner, A.J.; Overeem, I.; Hutton, E.W.H.; Hannon, M.T.; Brakenridge, G.R.; Day, J.; Vörösmarty, C.; Saito, Y.; Giosan, L.; et al. Sinking deltas due to human activities. *Nat. Geosci.* **2009**, *2*, 681–686. [CrossRef]
5. Syvitski, J.; Ángel, J.R.; Saito, Y.; Overeem, I.; Vörösmarty, C.J.; Wang, H.; Olago, D. Earth's sediment cycle during the Anthropocene. *Nat. Rev. Earth Environ.* **2022**, *3*, 179–196. [CrossRef]
6. Anthony, E.; Syvitski, J.; Săinescu, F.; Nicholls, R.J.; Cohen, K.M.; Marriner, N.; Saito, Y.; Day, J.; Minderhoud, P.S.J.; Amorosi, A.; et al. Delta sustainability from the Holocene to the Anthropocene and envisioning the future. *Nat. Sustain.* **2024**, *7*, 1235–1246. [CrossRef]
7. Syvitski, J.; Vörösmarty, C.J.; Kettner, A.J.; Green, P. Impact of Humans on the Flux of Terrestrial Sediment to the Global Coastal Ocean. *Science* **2005**, *308*, 376–380. [CrossRef]
8. Gupta, H.; Kao, S.-J.; Dai, M. The role of mega dams in reducing sediment fluxes: A case study of large Asian rivers. *J. Hydrol.* **2012**, *464–465*, 447–458. [CrossRef]
9. Shen, Z.; Rosenheim, B.E.; Törnqvist, T.E.; Lang, A. Engineered Continental-Scale Rivers Can Drive Changes in the Carbon Cycle. *AGU Adv.* **2021**, *2*, e2020AV000273. [CrossRef]
10. Bianchi, T.S.; Mayer, L.M.; Amaral, J.H.F.; Arndt, S.; Galy, V.; Kemp, D.B.; Kuehl, S.A.; Murray, N.J.; Regnier, P. Anthropogenic impacts on mud and organic carbon cycling. *Nat. Geosci.* **2024**, *17*, 287–297. [CrossRef]
11. Chen, D.; Li, X.; Saito, Y.; Liu, J.P.; Duan, Y.; Liu, S.; Zhang, L. Recent evolution of the Irrawaddy (Ayeyarwady) Delta and the impacts of anthropogenic activities: A review and remote sensing survey. *Geomorphology* **2020**, *365*, 107231. [CrossRef]
12. Keil, R. Anthropogenic Forcing of Carbonate and Organic Carbon Preservation in Marine Sediments. *Annu. Rev. Mar. Sci.* **2017**, *9*, 151–172. [CrossRef] [PubMed]
13. Bianchi, T.S.; Cui, X.; Blair, N.E.; Burdige, D.J.; Eglinton, T.I.; Galy, V. Centers of organic carbon burial and oxidation at the land-ocean interface. *Org. Geochem.* **2018**, *115*, 138–155. [CrossRef]
14. Blair, N.E.; Aller, R.C. The Fate of Terrestrial Organic Carbon in the Marine Environment. *Annu. Rev. Mar. Sci.* **2012**, *4*, 401–423. [CrossRef]

15. Hemingway, J.D.; Rothman, D.H.; Grant, K.E.; Rosengrad, S.Z.; Eglinton, T.I.; Derry, L.A.; Galy, V.V. Mineral Protection regulates long-term preservation of natural organic carbon. *Nature* **2019**, *570*, 228–231. [CrossRef]
16. Pszonka, J.; Žecová, K.; Wendorff, M. Oligocene turbidite fans of the Dukla Basin: New age data from the calcareous nannofossils and paleoenvironmental conditions (Cergowa beds, Polish–Slovakian borderland). *Geol. Carpathica* **2019**, *70*, 311–324. [CrossRef]
17. Bouchez, J.; Beyssac, O.; Galy, V.; Gaillardet, J.; France-Lanord, C.; Maurice, L.; Moreira-Turcq, P. Oxidation of petrogenic organic carbon in the Amazon floodplain as a source of atmospheric CO_2. *Geology* **2010**, *38*, 255–258. [CrossRef]
18. Wei, B.; Mollenhauer, G.; Kusch, S.; Hefter, J.; Grotheer, H.; Schefuß, E.; Geibert, W.; Ransby, D.; Jia, G. Anthropogenic Perturbations Change the Quality and Quantity of Terrestrial Carbon Flux to the Coastal Ocean. *J. Geophys. Res.-Biogeosci.* **2023**, *128*, e2023JG007482. [CrossRef]
19. Maavara, T.; Chen, Q.; Van Meter, K.; Brown, L.E.; Zhang, J.; Ni, J.; Zarfl, C. River dam impacts on biogeochemical cycling. *Nat. Rev. Earth Environ.* **2020**, *1*, 103–116. [CrossRef]
20. Valiela, I.; Bartholomew, M.; Giblin, A.; Tucker, J.; Harris, C.; Martinetto, P.; Otter, M.; Camilli, L.; Stone, T. Watershed Deforestation and Down-Estuary Transformations Alter Sources, Transport, and Export of Suspended Particles in Panamanian Mangrove Estuaries. *Ecosystems* **2014**, *17*, 96–111. [CrossRef]
21. Amoakwah, E.; Lucas, S.T.; Didenko, N.A.; Rahman, M.A.; Islam, K.R. Impact of deforestation and temporal land-use change on soil organic carbon storage, quality, and lability. *PLoS ONE* **2022**, *17*, e0263205. [CrossRef] [PubMed]
22. Wang, C.; Zhang, C.; Wang, Y.; Jia, G.; Wang, Y.; Zhu, C.; Yu, Q.; Zou, X. Anthropogenic perturbations to the fate of terrestrial organic matter in a river-dominated marginal sea. *Geochim. Cosmochim. Acta* **2022**, *333*, 242–262. [CrossRef]
23. Milliman, J.; Mie-e, R. Rivér Flux to the Sea: Impact of Human Intervention on River Systems and Adjacent Coastal Areas. In *Climate Change Impact on Coastal Habitation*, 1st ed.; CRC Press: Boca Raton, FL, USA, 1995; pp. 57–83.
24. Richards, D.R.; Friess, D.A. Rates and drivers of mangrove deforestation in Southeast Asia, 2000–2012. *Proc. Natl. Acad. Sci. USA* **2015**, *113*, 344–349. [CrossRef] [PubMed]
25. Jennerjahn, T.C.; Gilman, E.; Krauss, K.W.; Lacerda, L.D.; Nordhaus, I.; Wolanski, E. Mangrove Ecosystems under Climate Change. In *Mangrove Ecosystems: A Global Biogeographic Perspective*; Rivera-Monroy, V.H., Lee, S.Y., Kristensen, E., Twilley, R.R., Eds.; Springer: Cham, Switzerland, 2017; pp. 211–244.
26. Estoque, R.C.; Myint, S.W.; Wang, C.; Ishtiaque, A.; Aung, T.T.; Emerton, L.; Ooba, M.; Hijioka, Y.; Mon, M.S.; Wang, Z.; et al. Assessing environmental impacts and change in Myanmar's mangrove ecosystem service value due to deforestation (2000–2014). *Glob. Change Biol.* **2018**, *24*, 5391–5410. [CrossRef] [PubMed]
27. Torgersen, T.; Chivas, A.R. Terrestrial organic carbon in marine sediment: A preliminary balance for a mangrove environment derived from 13C. *Chem. Geol. Isot. Geosci.* **1985**, *52*, 379–390. [CrossRef]
28. Jennerjahn, T.C.; Ittekkot, V. Relevance of mangroves for the production and deposition of organic matter along tropical continental margins. *Sci. Nat.* **2002**, *89*, 23–30. [CrossRef]
29. Kristensen, E.; Bouillon, S.; Dittmar, T.; Marchand, C. Organic carbon dynamics in mangrove ecosystems: A review. *Aquat. Bot.* **2008**, *89*, 201–219. [CrossRef]
30. Alongi, D.M. Carbon sequestration in mangrove forests. *Carbon Manag.* **2012**, *3*, 313–322. [CrossRef]
31. Alongi, D.M. Carbon Cycling and Storage in Mangrove Forests. *Annu. Rev. Mar. Sci.* **2014**, *6*, 195–219. [CrossRef]
32. Arellano, A.R.; Bianchi, T.S.; Osburn, C.L.; D'Sa, E.J.; Ward, N.D.; Oviedo-Vargas, D.; Joshi, I.D.; Ko, D.S.; Shields, M.R.; Kurian, G.; et al. Mechanisms of Organic Matter Export in Estuaries with Contrasting Carbon Sources. *J. Geophys. Res.-Biogeosci.* **2019**, *124*, 3168–3188. [CrossRef]
33. Webb, E.L.; Jachowski, N.R.A.; Phelps, J.; Friess, D.A.; Than, M.M.; Ziegler, A.D. Deforestation in the Ayeyarwady Delta and the conservation implications of an internationally-engaged Myanmar. *Glob. Environ. Change* **2014**, *24*, 321–333. [CrossRef]
34. Atwood, T.B.; Connolly, R.M.; Almahasheer, H.; Carnell, P.E.; Duarte, C.M.; Ewers Lewis, C.J.; Irigoien, X.; Kelleway, J.J.; Lavery, P.S.; Macreadie, P.I.; et al. Global patterns in mangrove soil carbon stocks and losses. *Nat. Clim. Change* **2017**, *7*, 523–528. [CrossRef]
35. Gandhi, S.; Jones, T. Identifying Mangrove Deforestation Hotspots in South Asia, Southeast Asia and Asia-Pacific. *Remote Sens.* **2019**, *11*, 728. [CrossRef]
36. Richards, D.R.; Thompson, B.S.; Wijedasa, L. Quantifying net loss of global mangrove carbon stocks from 20 years of land cover change. *Nat. Commun.* **2020**, *11*, 4260. [CrossRef] [PubMed]
37. Alongi, D.M. Lateral Export and Sources of Subsurface Dissolved Carbon and Alkalinity in Mangroves: Revising the Blue Carbon Budget. *J. Mar. Sci. Eng.* **2022**, *10*, 1916. [CrossRef]
38. Blair, N.E.; Leithold, E.L.; Aller, R.C. From bedrock to burial: The evolution of particulate organic carbon across coupled watershed-continental margin systems. *Mar. Chem.* **2004**, *92*, 141–156. [CrossRef]
39. Baronas, J.J.; Stevenson, E.I.; Hackney, C.R.; Darby, S.E.; Bickle, M.J.; Hilton, R.G.; Larkin, C.S.; Parsons, D.R.; Myo Khaing, A.; Tipper, E.T. Integrating Suspended Sediment Flux in Large Alluvial River Channels: Application of a Synoptic Rouse-Based Model to the Irrawaddy and Salween Rivers. *J. Geophys. Res. Earth Surf.* **2020**, *125*, e2020JF005554. [CrossRef]

40. Kuehl, S.A.; Williams, J.; Liu, J.P.; Harris, C.; Aung, D.W.; Tarpley, D.; Goodwyn, M.; Aye, Y.Y. Sediment dispersal and accumulation off the Ayeyarwady delta—Tectonic and oceanographic controls. *Mar. Geol.* **2019**, *417*, 106000. [CrossRef]
41. Liu, J.P.; Kuehl, S.A.; Pierce, A.C.; Williams, J.; Blair, N.E.; Harris, C.K.; Aung, D.W.; Aye, Y.Y. Fate of Ayeyarwady and Thanlwin Rivers Sediments in the Andaman Sea and Bay of Bengal. *Mar. Geol.* **2020**, *423*, 106137. [CrossRef]
42. Flynn, E.R.; Kuehl, S.A.; Harris, C.K.; Fair, M.J. Sediment and terrestrial organic carbon budgets for the offshore Ayeyarwady Delta, Myanmar: Establishing a baseline for future change. *Mar. Geol.* **2022**, *447*, 106782. [CrossRef]
43. Harris, C.K.; Wacht, J.T.; Fair, M.J.; Côté, J.M. ADCP Observations of Currents and Suspended Sediment in the Macrotidal Gulf of Martaban, Myanmar. *Front. Earth Sci.* **2022**, *10*, 820326. [CrossRef]
44. Damodararao, K.; Singh, S.K.; Rai, V.K.; Ramaswamy, V.; Rao, P.S. Lithology, Monsoon and Sea-Surface Current Control on Provenance, Dispersal and Deposition of Sediments over the Andaman Continental Shelf. *Front. Mar. Sci.* **2016**, *3*, 118. [CrossRef]
45. IOC; IHO; BODC. *"Centenary Edition of the GEBCO Digital Atlas", Published on CDROM on Behalf of the Intergovernmental Oceanographic Commission and the International Hydrographic Organization as Part of the General Bathymetric Chart of the Oceans*; British Oceanographic Data Centre: Liverpool, UK, 2023.
46. Glover, H.E.; Ogston, A.S.; Fricke, A.T.; Nittrouer, C.A.; Aung, C.; Naing, T.; Kyu Kyu, K.; Htike, H. Connecting Sediment Retention to Distributary-Channel Hydrodynamics and Sediment Dynamics in a Tide-dominated Delta: The Ayeyarwady Delta, Myanmar. *J. Geophys. Res. Earth Surf.* **2021**, *126*, e2020JF005882. [CrossRef]
47. Grill, G.; Lehner, B.; Thieme, M.; Geenen, B.; Tickner, D.; Antonelli, F.; Babu, S.; Borrelli, P.; Cheng, L.; Crochetiere, H.; et al. Mapping the world's free-flowing rivers. *Nature* **2019**, *569*, 215–221. [CrossRef]
48. Anthony, E.J.; Besset, M.; Dussouillez, P.; Goichot, M.; Loisel, H. Overview of the Monsoon-influenced Ayeyarwady River delta, and delta shoreline mobility in response to changing fluvial sediment supply. *Mar. Geol.* **2019**, *417*, 106038. [CrossRef]
49. Rodolfo, K.S. Sediments of the Andaman Basin, northeastern Indian Ocean. *Mar. Geol.* **1969**, *7*, 371–402. [CrossRef]
50. Fair, M. Sediment Transport and Trapping on the Ayeyarwady-Martaban Continental Shelf. Master's Thesis, Virginia Institute of Marine Science, Gloucester Point, VA, USA, 2021.
51. Ramaswamy, V.; Rao, P.S.; Rao, K.H.; Thwin, S.; Rao, N.S.; Raiker, V. Tidal influence on suspended sediment distribution and dispersal in the northern Andaman Sea and Gulf of Martaban. *Mar. Geol.* **2004**, *208*, 33–42. [CrossRef]
52. Bender, F.; Bannert, D.; Bannert, D.N. *Geology of Burma*; Gebr. Borntraeger: Berlin, Germany, 1983.
53. Stamp, L.D. The Irrawaddy River. *Geogr. J.* **1940**, *95*, 329–352. [CrossRef]
54. Bertrand, G.; Rangin, C. Tectonics of the western margin of the Shan plateau (central Myanmar): Implication for the India–Indochina oblique convergence since the Oligocene. *J. Asian Earth Sci.* **2003**, *21*, 1139–1157. [CrossRef]
55. Mitchell, A.H.G.; Htay, M.T.; Htun, K.M.; Win, M.N.; Oo, T.; Hlaing, T. Rock relationships in the Mogok metamorphic belt, Tatkon to Mandalay, central Myanmar. *J. Asian Earth Sci.* **2007**, *29*, 891–910. [CrossRef]
56. Chapman, H.; Bickle, M.; Thaw, S.H.; Thiam, H.N. Chemical fluxes from time series sampling of the Irrawaddy and Salween Rivers, Myanmar. *Chem. Geol.* **2015**, *401*, 15–27. [CrossRef]
57. Garzanti, E.; Wang, J.-G.; Vezzoli, G.; Limonta, M. Tracing provenance and sediment fluxes in the Irrawaddy River basin (Myanmar). *Chem. Geol.* **2016**, *440*, 73–90. [CrossRef]
58. Hossain, H.M.Z.; Kawahata, H.; Roser, B.P.; Sampei, Y.; Manaka, T.; Otani, S. Geochemical characteristics of modern river sediments in Myanmar and Thailand: Implications for provenance and weathering. *Geochemistry* **2017**, *77*, 443–458. [CrossRef]
59. Giosan, L.; Naing, T.; Min Tun, M.; Clift, P.D.; Filip, F.; Constantinescu, S.; Khonde, N.; Blusztajn, J.; Buylaert, J.P.; Stevens, T.; et al. On the Holocene evolution of the Ayeyawady megadelta. *Earth Surf. Dyn.* **2018**, *6*, 451–466. [CrossRef]
60. Ketelsen, T.; Taylor, L.; Vinh, M.K.; Hunter, R.; Johnston, R.; Liu, S.; Tint, K.; Gyi, K.M.M.; Charles, M. *State of Knowledge: River Health in the Ayeyarwady*; International Water Management Institute (IWMI): Colombo, Sri Lanka, 2017.
61. Vogel, A.; Seeger, K.; Brill, D.; Brückner, H.; Soe, K.K.; Oo, N.W.; Aung, N.; Myint, Z.N.; Kraas, F. Identifying Land-Use Related Potential Disaster Risk Drivers in the Ayeyarwady Delta (Myanmar) during the Last 50 Years (1974–2021) Using a Hybrid Ensemble Learning Model. *Remote Sens.* **2022**, *14*, 3568. [CrossRef]
62. Gruel, C.R.; Latrubesse, E.M. A Monitoring System of Sand Mining in Large Rivers and Its Application to the Ayeyarwady (Irrawaddy) River, Myanmar. *Water* **2021**, *13*, 2331. [CrossRef]
63. De Alban, J.D.T.; Jamaludin, J.; Wong De Wen, D.; Than, M.M.; Webb, E.L. Improved estimates of mangrove cover and change reveal catastrophic deforestation in Myanmar. *Environ. Res. Lett.* **2020**, *15*, 034034. [CrossRef]
64. Aye, W.N.; Tong, X.; Tun, A.W. Species Diversity, Biomass and Carbon Stock Assessment of Kanhlyashay Natural Mangrove Forest. *Forests* **2022**, *13*, 1013. [CrossRef]
65. Hennig, T. Damming the transnational Ayeyarwady basin. Hydropower and the water-energy nexus. *Renew. Sustain. Energy Rev.* **2016**, *65*, 1232–1246. [CrossRef]
66. Searle, M.P.; Windley, B.F.; Coward, M.P.; Cooper, D.J.W.; Rex, A.J.; Rex, D.; Tingdong, L.; Xuchang, X.; Jan, M.Q.; Thakur, V.C.; et al. The closing of Tethys and the tectonics of the Himalaya. *Geol. Sci. Am. Bull.* **1987**, *98*, 678–701. [CrossRef]
67. Ramaswamy, V.; Rao, P.S. *The Myanmar Continental Shelf*; The Geological Society of London: London, UK, 2014.

68. Awasthi, N.; Ray, J.S.; Singh, A.K.; Band, S.T.; Rai, V.K. Provenance of the Late Quaternary sediments in the Andaman Sea: Implications for monsoon variability and ocean circulation. *Geochem. Geophys. Geosyst.* **2014**, *15*, 3890–3906. [CrossRef]
69. Robinson, R.A.J.; Bird, M.I.; Oo, N.W.; Hoey, T.B.; Aye, M.M.; Higgitt, D.L.; Lu, X.X.; Swe, A.; Tun, T.; Win, S.L. The Irrawaddy River Sediment Flux to the Indian Ocean: The Original Nineteenth-Century Data Revisited. *J. Geol.* **2007**, *115*, 629–640. [CrossRef]
70. Johnston, R.; McCartney, M.; Liu, S.; Ketelsen, T.; Taylor, L.; Vinh, M.K.; Gyi, M.K.K.; Aung, T.; Gyi, K.M.M. *State of Knowledge: River Health in the Salween*; International Water Management Institute (IWMI): Colombo, Sri Lanka, 2017.
71. Fung, Z.; Lamb, V. Dams, Diversions, and Development: Slow Resistance and Authoritarian Rule in the Salween River Basin. *Antipode* **2023**, *55*, 1662–1685. [CrossRef]
72. Gardiner, N.J.; Robb, L.J.; Searle, M.P. The metallogenic provinces of Myanmar. *Appl. Earth Sci.* **2014**, *123*, 25–38. [CrossRef]
73. Khin, K.; Sakai, T.; Zaw, K. Arakan Coastal Ranges in western Myanmar, geology and provenance of Neogene siliciclastic sequences: Implications for the tectonic evolution of the Himalaya–Bengal System. In *Geological Society, London, Memoirs*; Lyell Collection: London, UK, 2017; Volume 48, pp. 81–116.
74. Hedley, P.J.; Bird, M.I.; Robinson, R.A.J. Evolution of the Irrawaddy delta region since 1850: Evolution of the Irrawaddy delta region since 1850. *Geogr. J.* **2009**, *176*, 138–149. [CrossRef]
75. Rao, P.S.; Ramaswamy, V.; Thwin, S. Sediment texture, distribution and transport on the Ayeyarwady continental shelf, Andaman Sea. *Mar. Geol.* **2005**, *216*, 239–247. [CrossRef]
76. Colin, C.; Turpin, L.; Bertaux, J.; Desprairies, A.; Kissel, C. Erosional history of the Himalayan and Burman ranges during the last two glacial–interglacial cycles. *Earth Planet. Sci. Lett.* **1999**, *171*, 647–660. [CrossRef]
77. Licht, A.; France-Lanord, C.; Reisberg, L.; Fontaine, C.; Soe, A.N.; Jaeger, J.J. A palaeo Tibet–Myanmar connection? Reconstructing the Late Eocene drainage system of central Myanmar using a multi-proxy approach. *J. Geol. Soc.* **2013**, *170*, 929–939. [CrossRef]
78. Sommerfield, C.K.; Nittrouer, C.A.; Alexander, C.R. 7Be as a tracer of flood sedimentation on the northern California continental margin. *Cont. Shelf Res.* **1999**, *19*, 335–361. [CrossRef]
79. Yu, M.; Eglinton, T.I.; Haghipour, N.; Montluçon, D.B.; Wacker, L.; Wang, Z.; Jin, G.; Zhao, M. Molecular isotopic insights into hydrodynamic controls on fluvial suspended particulate organic matter transport. *Geochim. Cosmochim. Acta* **2019**, *262*, 78–91. [CrossRef]
80. Fagerlund, G. Determination of specific surface by the BET method. *Mater. Struct.* **1973**, *6*, 239–245. [CrossRef]
81. Keiser, L.; Soreghan, G.S.; Joo, Y.J. Effects Of Drying Techniques on Grain-Size Analyses of Fine-Grained Sediment. *J. Sediment. Res.* **2014**, *84*, 893–896. [CrossRef]
82. Fontugne, M.; Duplessy, J.C. Carbon isotope ratio of marine plankton related to surface water masses. *Earth Planet. Sci. Lett.* **1978**, *41*, 365–371. [CrossRef]
83. Bird, M.; Robinson, R.; Oo, N.W.; Aye, M.M.; Lu, X.; Higgitt, D.; Swe, A.; Tun, T.; Win, S.L.; Aye, K.S.; et al. A preliminary estimate of organic carbon transport by the Ayeyarwady (Irrawaddy) and Thanlwin (Salween) Rivers of Myanmar. *Quat. Int.* **2008**, *186*, 113–122. [CrossRef]
84. Lamb, A.L.; Wilson, G.P.; Leng, M.J. A review of coastal palaeoclimate and relative sea-level reconstructions using $\delta^{13}C$ and C/N ratios in organic material. *Earth-Sci. Rev.* **2006**, *75*, 29–57. [CrossRef]
85. Gaye-Haake, B.; Lahajnar, N.; Emeis, K.C.; Unger, D.; Rixen, T.; Suthhof, A.; Ramaswamy, V.; Schulz, H.; Paropkari, A.L.; Guptha, M.V.S.; et al. Stable nitrogen isotopic ratios of sinking particles and sediments from the northern Indian Ocean. *Mar. Chem.* **2005**, *96*, 243–255. [CrossRef]
86. Perdue, E.M.; Koprivnjak, J.F. Using the C/N ratio to estimate terrigenous inputs of organic matter to aquatic environments. *Estuar. Coast. Shelf Sci.* **2007**, *73*, 65–72. [CrossRef]
87. Ramaswamy, V.; Gaye, B.; Shirodkar, P.; Rao, P.; Chivas, A.; Wheeler, D.; Thwin, S. Distribution and sources of organic carbon, nitrogen and their isotopic signatures in sediments from the Ayeyarwady (Irrawaddy) continental shelf, northern Andaman Sea. *Mar. Chem.* **2008**, *111*, 137–150. [CrossRef]
88. Pinti, D.L.; Hashizume, K. Early Life Record from Nitrogen Isotopes. In *Earliest Life on Earth: Habitats, Environments and Methods of Detection*; Golding, S.D., Glikson, M., Eds.; Springer: Dordrecht, The Netherlands, 2011; pp. 183–205.
89. Hossain, M.S.; Sarker, S.; Sharifuzzaman, S.M.; Chowdhury, S.R. Primary productivity connects hilsa fishery in the Bay of Bengal. *Sci. Rep.* **2020**, *10*, 5659. [CrossRef]
90. Lin, B.; Liu, Z.; Eglinton, T.I.; Kandasamy, S.; Blattmann, T.M.; Haghipour, N.; Huang, K.F.; You, C.F. Island-wide variation in provenance of riverine sedimentary organic carbon: A case study from Taiwan. *Earth Planet. Sci. Lett.* **2020**, *539*, 116238. [CrossRef]
91. Aller, R.C.; Blair, N.E. Carbon remineralization in the Amazon–Guianas tropical mobile mudbelt: A sedimentary incinerator. *Cont. Shelf Res.* **2006**, *26*, 2241–2259. [CrossRef]
92. Yao, P.; Zhao, B.; Bianchi, T.S.; Guo, Z.; Zhao, M.; Li, D.; Pan, H.; Wang, J.; Zhang, T.; Yu, Z. Remineralization of sedimentary organic carbon in mud deposits of the Changjiang Estuary and adjacent shelf: Implications for carbon preservation and authigenic mineral formation. *Cont. Shelf Res.* **2014**, *91*, 1–11. [CrossRef]

93. Kuehl, S.A.; Pacioni, T.D.; Rine, J.M. Seabed dynamics of the inner Amazon continental shelf: Temporal and spatial variability of surficial strata. *Mar. Geol.* **1995**, *125*, 283–302. [CrossRef]
94. Martin, D.P.; Nittrouer, C.A.; Ogston, A.S.; Crockett, J.S. Tidal and seasonal dynamics of a muddy inner shelf environment, Gulf of Papua. *J. Geophys. Res. Earth Surf.* **2008**, *113*, F01S07. [CrossRef]
95. Aller, R.C.; Blair, N.E.; Xia, Q.; Rude, P.D. Remineralization rates, recycling, and storage of carbon in Amazon shelf sediments. *Cont. Shelf Res.* **1996**, *16*, 753–786. [CrossRef]
96. Aller, R.C. Mobile deltaic and continental shelf muds as suboxic, fluidized bed reactors. *Mar. Chem.* **1998**, *61*, 143–155. [CrossRef]
97. Zhao, B.; Yao, P.; Bianchi, T.S.; Arellano, A.R.; Wang, X.; Yang, J.; Su, R.; Wang, J.; Xu, Y.; Huang, X.; et al. The remineralization of sedimentary organic carbon in different sedimentary regimes of the Yellow and East China Seas. *Chem. Geol.* **2018**, *495*, 104–117. [CrossRef]
98. Bao, R.; Zhao, M.; McNichol, A.; Galy, V.; McIntyre, C.; Haghipour, N.; Eglinton, T.I. Temporal constraints on lateral organic matter transport along a coastal mud belt. *Org. Geochem.* **2019**, *128*, 86–93. [CrossRef]
99. Bridgestock, L.; Henderson, G.M.; Holdship, P.; Khaing, A.M.; Naing, T.T.; Myint, T.A.; Htun, W.W.; Khant, W.; Thu, W.M.; Chi, M.A.N.; et al. Dissolved trace element concentrations and fluxes in the Irrawaddy, Salween, Sittaung and Kaladan Rivers. *Sci. Total Environ.* **2022**, *841*, 156756. [CrossRef]
100. Nyunt, T.; Moe, A.; Zaya, K.; Sone, S. Some critical mineral and element occurrences and potential in Myanmar. *Thai Geosci. J.* **2023**, *4*, 11–32.
101. Vinayachandran, P.N.; Shetye, S.R.; Sengupta, D.; Gadgil, S. Forcing mechanisms of the Bay of Bengal circulation. *Curr. Sci. India* **1996**, *71*, 753–763.
102. Hacker, P.; Firing, E.; Hummon, J.; Gordon, A.L.; Kindle, J.C. Bay of Bengal currents during the Northeast Monsoon. *Geophys. Res. Lett.* **1998**, *25*, 2769–2772. [CrossRef]
103. Kim, H.T.; Kim, J.G. Heavy Metal Concentrations in the Mollusc Gastropod, Cipangopaludina chinensis malleata from Upo Wetland Reflect the Level of Heavy Metals in the Sediments. *J. Ecol. Environ.* **2006**, *29*, 453–460. [CrossRef]
104. Qi, L.; Wu, Y.; Chen, S.; Wang, X. Evaluation of Abandoned Huanghe Delta as an Important Carbon Source for the Chinese Marginal Seas in Recent Decades. *J. Geophys. Res.-Oceans* **2021**, *126*, e2020JC017125. [CrossRef]
105. Li, W.; Li, X.; Zhao, X.; Sun, C.; Nie, T.; Hu, Y.; Wang, C. Impacts of Climate Change and Human Perturbations on Organic Carbon Burial in the Pearl River Estuary Over the Last Century. *Front. Mar. Sci.* **2022**, *9*, 848757. [CrossRef]
106. Allison, M.A.; Nittrouer, C.A.; Ogston, A.S.; Mullarney, J.C.; Nguyen, T.T. Sedimentation and Survival of the Mekong Delta: A Case Study of Decreased Sediment Supply and Accelerating Rates of Relative Sea Level Rise. *Oceanography* **2017**, *30*, 98–109. [CrossRef]
107. Le, T.P.Q.; Le, N.D.; Dao, V.N.; Rochelle-Newall, E.; Nguyen, T.M.H.; Marchand, C.; Duong, T.T.; Phung, T.X.B. Change in carbon flux (1960–2015) of the Red River (Vietnam). *Environ. Earth Sci.* **2018**, *77*, 658. [CrossRef]
108. Le, N.D.; Le, T.P.Q.; Phung, T.X.B.; Duong, T.T.; Didier, O. Impact of hydropower dam on total suspended sediment and total organic nitrogen fluxes of the Red River (Vietnam). *Proc. Int. Assoc. Hydrol. Sci.* **2020**, *383*, 367–374. [CrossRef]
109. Li, D.; Yao, P.; Bianchi, T.S.; Zhang, T.; Zhao, B.; Pan, H.; Wang, J.; Yu, Z. Organic carbon cycling in sediments of the Changjiang Estuary and adjacent shelf: Implication for the influence of Three Gorges Dam. *J. Mar. Syst.* **2014**, *139*, 409–419. [CrossRef]
110. Liu, Y.; Deng, B.; Du, J.; Zhang, G.; Hou, L. Nutrient burial and environmental changes in the Yangtze Delta in response to recent river basin human activities. *Environ. Pollut.* **2019**, *249*, 225–235. [CrossRef]
111. Lu, T.; Wang, H.; Wu, X.; Bi, N.; Hu, L.; Bianchi, T.S. Transport of particulate organic carbon in the lower Yellow River (Huanghe) as modulated by dam operation. *Glob. Planet. Change* **2022**, *217*, 103948. [CrossRef]